Investigation of Network Heterogeneities in Filled, Trimodal, Highly Functional PDMS Networks by ^{1}H Multiple Quantum NMR

Erica Gjersing,[||] Sarah Chinn,[†] Jason R. Giuliani,[†] Julie Herberg,[†] Robert S. Maxwell,*[,†] Eric Eastwood,[‡] Dan Bowen,[‡] and Tom Stephens[§]

Lawrence Livermore National Laboratory, 7000 East Ave, Livermore, California 94551, Honeywell Federal Manufacturing and Technologies Plant, Kansas City, Missouri, Los Alamos National Laboratory, Los Alamos, New Mexico, and Department of Chemical Engineering and Materials Science, University of California, Davis, Davis, California

Received September 8, 2006; Revised Manuscript Received April 5, 2007

ABSTRACT: The segmental order and dynamics of polymer network chains in a filled, trimodal silicone foam network have been studied by static ^{1}H multiple quantum (MQ) NMR methods to gain insight into the structure property relationships. The foam materials were synthesized with two different types of cross-links, with functionalities, ϕ, of 4 and near 60. The network chains were composed of distributions of high, low, and medium molecular weight chains. Cross-linking was accomplished by standard acid-catalyzed reactions. MQ NMR methods have detected domains with residual dipolar couplings ($\langle\Omega_d\rangle$) of near 4 and 1 krad/s assigned to (a) the shorter polymer chains and chains near the multifunctional ($\phi = 60$) cross-linking sites and to (b) the longer polymer chains far from these sites. Three structural variables were systematically varied and the mechanical properties via compression and distributions of residual dipolar couplings measured in order to gain insight into the network structural motifs that contribute significantly to the composite properties. The partitioning and average values of the residual dipolar couplings for the two domains were observed to be dependent on formulation variables and provided increased insight into the network structure of these materials which are unavailable from swelling and spin-echo methods. The results of this study suggest that the domains with high cross-link density contribute significantly to the high strain modulus, while the low cross-link density domains do not. This is in agreement with theories and experimental studies on silicone bimodal networks over the last 20 years. In situ MQ-NMR of swollen samples suggests that the networks deform heterogeneously and nonaffinely. The heterogeneity of the deformation process was observed to depend on the amount of the high functionality cross-linking site PMHS. The NMR experiments shown here provide increased ability to characterize multimodal networks of typical engineering silicone foam materials and to gain significant insight into structure−property relationships.

Introduction

It is generally accepted that the bulk mechanical and relaxation properties of polymeric materials and their age dependence are controlled by the network structure.[1−6] In order to interpret mechanical properties such as modulus, strength, and toughness and to predict the time dependent changes in these properties, detailed characterization of the network structure and knowledge of the effect of structural changes on engineering properties have to be obtained. The degree and type of cross-linking, the molecular weight between cross-links, and the number of elastically ineffective chains (loops, dangling chain ends, sol-fraction), as well as filler content, surface properties, and interaction energies with the polymer network, must be characterized. In certain cases (e.g., solid elastomers constructed of model networks constructed from end linking reactions without the presence of filler) significant insight into the contributions of network structural parameters to material mechanical properties can be inferred from tensile stress−strain curves.[7−13] The required level of characterization can be difficult, however, to obtain for typical porous engineering silicone (often hydrogen blown) foams with complex structure (distributions of network chain lengths, highly functional cross-linking sites, and inorganic reinforcing fillers) used in compression. The characterization of cross-linked elastomeric foams by compression testing is hampered by large error bars and the lack of robust theories connecting compression modulus to network structure. There is in general a need to develop methods to characterize foamed elastomeric materials nondestructively.

NMR methods have shown increasing ability to characterize elastomer network structure and heterogeneities and, in fact, have gained much attention in the past few decades for their ability to characterize changes in chemical composition and network structure nondestructively.[14−37]A range of NMR experimental methods have been used to investigate segmental dynamics in, for example, silicone based elastomeric materials, and in fact, the use of ^{1}H relaxometry has become quite standard. Unfortunately, standard echo based relaxation methods have been shown to suffer from severe limitations.[17,26−30] Traditionally, relaxation times are interpreted in the context of the Anderson−Weiss model which assumes slow fluctuations of the residual dipolar couplings and that the rapid segmental dynamics are too fast to affect the relaxation times. The applicability of these assumptions have recently been called into question in a series of articles by Saalwächter.[30] It is the conclusion of these reports that the interpretation of relaxometry data to extract knowledge of the network chain segmental dynamics and the network structure are strongly dependent on assumptions that are not broadly applicable and are subject to artifacts relating to fitting parameters that can be highly interdependent.[26] Further, it has been shown, in some cases—including filled and cross-linked PDMS composites—that internal voids within the sample can create magnetic field

* Corresponding author. Telephone: (925) 423-4991. Fax: (925) 423-3720. E-mail: Maxwell7@llnl.gov.
[†] Lawrence Livermore National Laboratory.
[‡] Honeywell Federal Manufacturing and Technologies Plant.
[§] Los Alamos National Laboratory.
[||] Department of Chemical Engineering and Materials Science, University of California, Davis.

10.1021/ma0620924 CCC: $37.00
Published on Web 06/07/2007

gradients that interfere with the refocusing of transverse magnetization by spin-echoes.[23] A number of methods have been developed to bypass these limitations and include the dipolar correlation effect on the stimulated echo, the magic echo, and ^{2}H NMR line shape analysis.[19,21,24,25]

Recently ^{1}H multiple quantum (MQ) methods have been applied to the problem of characterizing structural and dynamic processes in elastomeric systems and have shown much promise for such applications.[22,23,26−37] Static ^{1}H multiple quantum NMR methods were initially shown to be applicable to elastomers by Schneider et al. and have been shown to more accurately quantitate the residual dipolar couplings reflective of network topology as well as provide qualitative access to distributions in the residual dipolar couplings, $\langle\Omega_d\rangle$, in silicone materials.[26−32,34] In elastomeric materials, $\langle\Omega_d\rangle$s are the result of topological constraints interfering with fast reorientations on the NMR time scale that otherwise would be expected to average homonuclear dipolar couplings to zero.[17] $\langle\Omega_d\rangle$s, in fact, have been shown to be quite sensitive to network and morphological changes and have been used to test theories of polymer structure, ordering, and dynamics.[17,26−30,34] It has been reported that the characterization of the growth of multiple quantum coherences can provide detailed insight into silicone network structure by increasing the selectivity of the NMR experiment to the structure most connected to the topology of the polymer network, including chain ordering at the surface of inorganic filler particles.[22,23,26−31] The MQ methods, in fact, have been shown to more accurately characterize the network structure than more traditional spin-echo-based approaches which can overestimate the residual dipolar couplings due to the inadequacies of the assumptions underlying the interpretation and/or effects of magnetic susceptibilities and field gradients.[26−30]

We have employed recently developed MQ methods to investigate the structure−property relationships in a series of trimodal, end-linked filled-PDMS networks cross-linked with highly functional silane sites. The general enhancements of mechanical properties through the use of multimodal distributions of chain lengths and the use of highly functional cross-linking agents have been described elsewhere.[4,6,7−13] The materials studied here are constructed from poly(dimethylsiloxane) (PDMS) chains of three average chain lengths, cross-linked with tetrapropoxysilane (TPS; functionality, ϕ, of four) and poly(methylhydrogensilane) (PMHS; $\phi = 30-80$), using standard condensation reactions.[38] Previous studies have demonstrated the ability of MQ NMR methods to characterize network structure in bimodal silicon networks, and in complex commercial silicone formulations.[22,23,26−28] The former networks are relatively simple compared to the materials studied here and used only cross-linking sites with $\phi = 3$ or 4. The commercial silicones studied previously were proprietary formulations and thus specific correlations between chemical formulation and network structure could not be obtained. Our results clearly demonstrate that these MQ methods can provide key insight into highly complex silicone networks and can be used to gain insight into the structure−function relationships unavailable by other means.

Experimental Section

Materials. Model silicone networks were produced using standard Sn−octanoate catalyzed, end-linking silicone chemistry.[38] The networks were constructed from a combination of hydroxyl-end-linked PDMS with three different average molecular weights [high molecular weight (HMW), $M_n = 13\,600$, $M_w = 58\,300$; medium molecular weight (MMW), $M_n = 11\,700$, $M_w = 27\,400$; low molecular weight (LMW), $M_n = 1530$, $M_w = 1850$] and two different cross-linking units [tetrapropoxysilane (TPS), FW = 264 g/mol, $\phi = 4$; poly(methylhydrogensilane) (PMHS)] of four different molecular weights ($M_n = 3700$, $M_w = 8200$, $\phi = 80$; $M_n = 3700$, $M_w = 8200$, $\phi = 70$; $M_n = 3700$, $M_w = 8200$, $\phi = 60$; $M_n = 2000$, $M_w = 4400$, $\phi = 30$). Here the functionality of the cross-linking sites, ϕ, is the number of available sites per molecule for crosslinking. In addition, diphenylmethylsilanol (DPMS: FW = 214 g/mol, $\phi = 1$) was added as a blowing agent and low-temperature modifier. All the above materials were obtained from NuSil [Carpenteria, CA].

The base resin was made by mixing all three hydroxyl-end-linked PDMS chains, diatomaceous earth filler [15 wt %], TPS [5 wt %], DPMS [5 wt %], and PMHS [2−6 wt %] with a mechanical mixer until homogeneous. Network foams were created by adding 5% by weight Sn−octanoate catalyst to the base resin at room temperature and mixing for approximately 15 s. The catalyzed resin was then immediately poured into the mold, closed, and allowed to cure for a minimum of 15 min. The reaction of the silanol sites of the PDMS chains with the silane sites on the PMHS produces H_2 which forms the pore structure as the network cures. The foamed network was then allowed to air cure at room temperature for a minimum of 16 h followed by postcuring at 240 °F for 3 to 3.5 h. The chemical species and an illustration of the resulting network are shown in Figure 1.

Materials were created for three studies: (1) the total weight of HO−PDMS−OH was kept the same, but the amount of the high MW chains was varied (essentially changing only the ratio of HMW to LMW and MMW chains and not the total amount of PDMS in the network); (2) the proportions of the three chain lengths of PDMS were kept constant and the amount of PMHS ($\phi = 60$) was varied; (3) the MW, and thus the length and functionality of the PMHS, was varied. Compositions for all samples studied here are listed in Table 1.

To further classify the networks, the average stoichiometry was calculated. The stoichiometery number is the ratio of available silanol end-links to the number of cross-link sites. Ideal networks would have a stoichiometry near one. However, many complex engineering silicones are characterized by stoichiometry values far from one, as may be required to meet specific formulation and engineering compliance requirements. For example, in the formation of blown foams such as these, a balance needs to be maintained between reaction rate and stoichiometry. There is a need to ensure that the reaction progresses at a sufficient rate to generate H_2 to a continuous pore structure, but not too rapid to generate a heterogeneous pore structure, and at the right rate to form a continuous network. Otherwise, a "good" foam might not be produced.

Methods. Swelling. Samples were weighed before and after swelling in toluene and the percent change in mass upon swelling was calculated. The average cross-link density of the polymer network can be related to the mass increase by methods described elsewhere.[20]

Mechanical Properties. The mechanical properties of the silicone foams were obtained using a custom built mechanical tester at the Kansas City Plant. Circular samples were molded with dimensions of 8.75 in. in diameter and 0.040 in. thick. Samples were tested in four test locations per sample pad by cycling to 550 kPa ± 50 kPa for four times with 40.5 ± 0.13 mm diameter platens. The reported values are the average over the four test locations on the fourth cycle averaged again over all samples tested (minimum of two, maximum of ten). In general, the variations in the measurements were ±12 kPa at 22% compression and ±70 kPa at 50% compression. The rate of loading and unloading were 0.021 ± 0.004 mm per second.

^{1}H NMR Methods. Experiments were performed at 400.13 MHz on a Bruker Avance 400 spectrometer using a Bruker TBI (HCX) 5 mm probe. In all cases, small (0.1 cm × 0.1 cm × 0.1 cm) pieces of elastomer were cut from a larger piece and set in the portion of a 5 mm NMR tube that would be within the coil volume of the probe. Traditional ^{1}H Hahn−spin-echo experiments[14,17,39] were performed with 90° pulse lengths of 5.75 μs and recycle delay time of 6 s, and echo delays were varied from 0 to 30 ms. Echo intensity

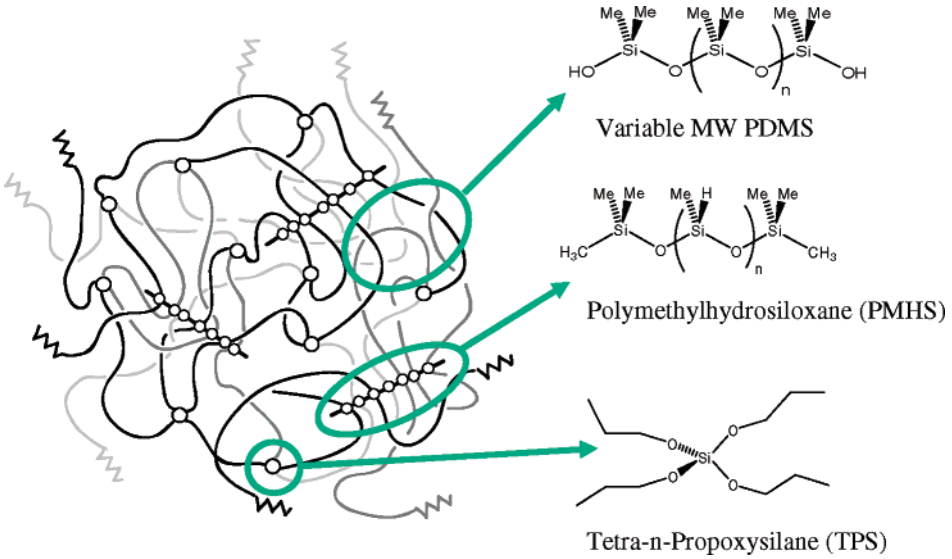

Figure 1. Illustration of the network structure and the starting materials used to formulate the networks studied here. Foams were prepared and characterized with varying amounts of PDMS with three MW distributions, with varying amounts of PMHS, and with PMHS with varying numbers of functional cross-linking sites, *n*.

Table 1. Composition of Foam Elastomers Studies Here[a]

	PDMS content study				PMHS content study					PMHS MW study			
	SX4	SX 462	SX 464	SX 466	SX2	SX3	SX 3.5	SX4	SX 4.5	LK 3626	LK short	LK DC	LK UCT
LMW−PDMS (wt %)	17.0	12.0	10.0	8.0	17.4	17.2	17.1	17.0	16.8	16.5	16.5	16.5	16.5
MMW−PDMS (wt %)	14.3	15.5	16.0	16.5	14.6	14.5	14.4	14.3	14.2	13.9	13.9	13.9	13.9
HMW−PDMS (wt %)	42.8	46.5	48.0	49.5	43.9	43.4	43.1	42.8	42.5	41.6	41.6	41.6	41.6
% HMW in total PMDS content	77.1	83.8	86.5	89.2	77.1	77.1	77.1	77.1	77.1	77.1	77.1	77.1	77.1
PMHS (wt %)	4.0	4.0	4.0	4.0	2.0	3.0	3.5	4.0	4.5	6.0	6.0	6.0	6.0
stoichiometric ratio SiH/SiOH	1.7	1.9	2	2.1	1.1	1.4	1.6	1.7	1.9	2.3	2.3	2.3	2.3
PMHS functionality (ϕ)	60	60	60	60	60	60	60	60	60	60	30	70	80
PMHS MW (g/mol)	8200	8200	8200	8200	8200	8200	8200	8200	8200	8200	4400	10 300	16 000

[a] In addition, all samples were made from 15 wt % diatomaceous earth, 5 wt % TPS, and 5 wt % DPMS as described above.

curves were plotted on a logarithmic scale and fit to a biexponential decay representing two separate relaxation processes:

$$\text{E.I.}(\tau) = X_{\text{short}} \exp(-2\,\tau\,/T_{2\text{short}}) + X_{\text{long}} \exp(-2\tau\,/T_{2\text{long}}) \quad (1)$$

where X_i are the mole fractions of chains in each domain, τ the delay between the 90 and 180° pulses, and $T_{2,i}$ are the transverse relaxation time of each domain. The domains with the short T_2 are typically assigned to the polymer chains associated with the cross-linked network while the domains with the long T_2 are assigned to the chains associated with the uncross-linked, sol-fraction.[18,20,21] For all the samples studied here, the amount of the sol-fraction (X_{long}) was found to be 4 ± 2% and the $T_{2\text{long}}$ was 12 ± 2 ms. Variable τ CPMG experiments were performed on a Bruker Optics minispec ProFiler. Echo decay curves were obtained with τs of 200 and 400 μs. The T_2 measured with τ = 400 μs was 22 ms while the T_2 measured for τ = 200 μs was 28 ms.

Multiple quantum NMR experiments were performed using the refocused multiple quantum excitation and reconversion pulse sequence shown in Figure 2.

The phases of the reconversion sequence were cycled in 90° steps with phase inversion on the observe pulse for coherence selections (the pulse sequence excites all even-multiple quantum coherences). CYCLOPS was then added to yield a 16 step phase cycle.[40] As described by Saalwächter et al., the pulse sequence yields the total sum of the even-multiple quantum coherences, dominated by the double quantum coherences, S_{mq}.[22,23,26−30] Pulse lengths of 5.75 μs were used with delay Δ_1 and Δ_2 equal to 4.7 μs and 5.8 μs respectively. The scaling factor, a, for these values is 0.655. The effective excitation time was then calculated by $t_e = ta$, where $t = 16\pi/2 + 8\Delta_1 + 8\Delta_2$.[26] Repeat experiments with longer delay times indicated that for these delays, no artifacts due to high duty cycle were observed. MQ growth experiments performed at temperatures of 300, 320, and 340 K were identical, indicating that the separation of timescales assumption was valid in these polymers.[26] In addition, repeat experiments with sample sizes of 10, 5, and 1 mm in diameter indicated that for sample sizes ≤5 mm sufficient RF homogeneity was obtained for the MQ experiments.

The spectral intensities from the MQ pulse sequence, $S_{\text{mq}}(t_e)$, were then normalized with the use of a reference spectrum obtained by removing the alternating phases on the observe pulse, $S_{\text{ref}}(t_e)$. The reference signal was then corrected by subtracting the long time decay component assigned to the sol-fraction of the polymer network, $S^*_{\text{ref}}(t_e) = S_{\text{ref}}(t_e) - S_{\text{ref-long}}(t_e)$.[26] The normalized multiple quantum integral was obtained by calculating the following for each effective excitation time, t_e,

$$I_{\text{mq}}(t_e) = S_{\text{mq}}(t_e)/(S_{\text{mq}}(t_e) + S^*_{\text{ref}}(t_e)) \quad (2)$$

This referencing method provides a growth curve that depends only on the network structure and not on the network structure and the dynamics. In the case of spins characterized by a dominant residual dipolar coupling, the multiple quantum growth curve is then described by

$$I_{\text{mq}}(t_e) = A(1 - \exp(-B\langle\Omega_d\rangle^2\, t_e^{\,2})) \quad (3)$$

In cases where spins can be described by more than one residual dipolar coupling, as in the case of bimodal or phase separated network structures, the multiple quantum growth curves can be described by a summation of growth curves based on a static second-moment approximation:

$$I_{\text{mq}}(t_e) = \Sigma\, 0.5X_i(1 - \exp(-B\,\langle\Omega_d\rangle_i^{\,2}\, t_e^{\,2}) \quad (4)$$

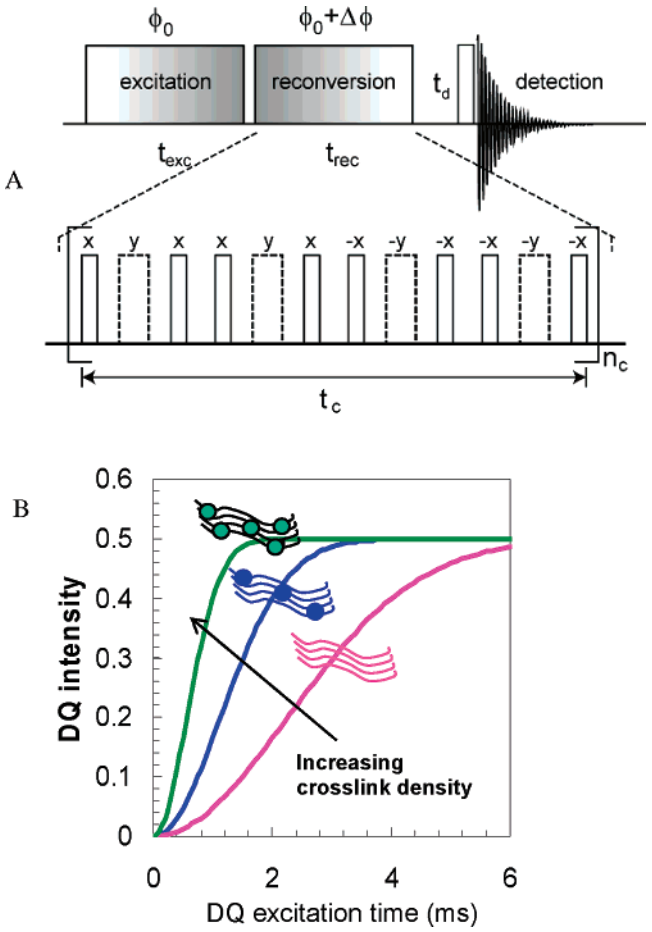

Figure 2. (A) ^{1}H MQ pulse sequence used in this study. Solid lines represent 90° pulses and dashed lines represent 180° pulses. The number of pulse trains, n_c, was incremented to generate growth curves. Phasing of the detection pulse was alternated to generate the reference curve. The raw growth curve and the reference data set were combined as discussed in the experimental section to generate growth curves that are dependent on cross-link density, as shown in part B.

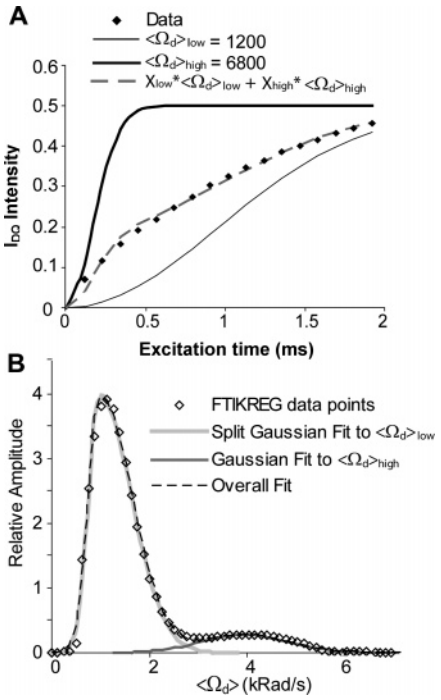

Figure 3. (A) MQ growth curve for pristine SX466 (diamonds) with biexponential fit (dashed line). Also shown are the normalized growth curves for the two domains that contribute to the biexponential fit. (B) Distribution of residual dipolar couplings $\langle\Omega_d\rangle$ obtained from FTIKREG regularization of the buildup curve in part A. Solid lines are the fits of Gaussian line shapes to the two overlapping distributions. Dashed line is the overall fit obtained by summing the two Gaussian distributions.

where X_i is the relative mole fraction of spins with $\langle\Omega_d\rangle_i$ (where $\langle\Omega_d\rangle^2 = (20/9)M_{2res}$, $A = 0.5$, and $B = (2/5)(2\pi)$,[2] and M_{2res} is the average residual second moment).[26,30]

The relationship between the residual dipolar coupling and polymer structural variables has been described using the scale-invariant model and extensively described elsewhere.[17,19,26,34,41] These studies have correlated the residual dipolar couplings to the dynamic order parameter, S_b, and to the number of statistical segments, N, between constraints averaged over all chains in the network:

$$S_b = [\langle\Omega_d\rangle/\langle\Omega_d\rangle_{static}]/\langle P_2(\cos\alpha)\rangle = 3\langle r^2/5N\rangle \quad (5)$$

where $\langle\Omega_d\rangle_{static}$ is the dipolar coupling in the absence of motion (but preaveraged by the fast motion of the methyl group) and equal to 8900 Hz, $\langle P_2(\cos\alpha)\rangle$ is the time averaged second-order Legendre polynomial of the angle between the dipolar vector and the chain axis (i.e., the angle between the chain axis and the Si−C vector, taken here to be 90°), and r is the vector describing the deviation of the end-to-end vector, **R**, from that of the unperturbed melt, $\mathbf{R}_o$: $r = \mathbf{R}/\mathbf{R}_o$.[39] The brackets on the right side of eq 5 indicate an average over all chains in the network.

Fitting and Regularization of Growth Curves. Two site fits of eq 4 for growth curves for $0 \le I_{mq}(t_e) \le 0.45$ were performed in MatLab (Mathworks) and the results are presented under the heading "2-Component Fit" in Table 2. Figure 3A shows a representative data curve, in solid diamonds, and the corresponding 2-site fit, in dashed light gray. Regularization of the buildup curves, also from 0 to 0.45, was performed using the FTIKREG software.[42] The probability distribution obtained from regularization is shown in Figure 3B as open diamonds. Using the program FitYK (http://www.unipress.waw.pl/fityk/), the first peak in the distributions was fit best with a split Gaussian function as given in equation 6:

$$y = a_0 \exp\left[-\ln(2)\left(\frac{x - a_1}{a_{2(3)}}\right)^2\right] \quad (6a)$$

$$y(x;a_0,a_1,a_2,a_3) = \begin{Bmatrix}\text{Gaussian}(x;a_0,a_1,a_2) & x \le a_1\\ \text{Gaussian}(x;a_0,a_1,a_3) & x > a_1\end{Bmatrix} \quad (6b)$$

The second peak was fit by a standard Gaussian as shown in Figure 3B. As has been mentioned elsewhere, due to the limitations with the finite signal-to-noise, the distributions obtained from the FTIKREG regularization procedure are only semiquantitative.[42]

Results and Discussion

As mentioned above, three sets of samples were synthesized for this study: 1) samples with varying ratios of the HMW PDMS chains to LMW and MMW PDMS chains; 2) samples with varying amounts of the highly functional cross-linking site PMHS; and 3) samples with varying molecular weight of the highly functional cross-linking site PMHS. These variables were chosen as likely contributors to changes in the mechanical properties of the materials. The compression stress−strain curves for three materials with varying amounts of high molecular weight chains to lower molecular weight chains are shown in Figure 4. The stress−strain curves are typical of engineering silicones with initial elastic behavior followed by a plateau range of strains in which the required load does not significantly increase with compression. At high strains the behavior is again elastic as the stress dramatically increases as foam network

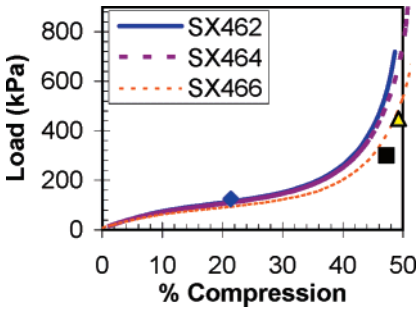

Figure 4. Loads required to reach given compressive strain for the materials studied here: (A) stress−strain curves for three samples in the HMW content study (solid, 83.9 wt %; dashed, 86.5 wt %; dotted, 89.2 wt %) with compressions of 22%, 47%, and 50% shown as diamonds, squares, and triangles, respectively.

reaches full density. The materials prepared here are approximately 30−40% porous; thus, the load at 20% compression is due to compression of foam structure, and differences between samples are due primarily to small differences in the porosity from sample to sample. At higher compressions, the foam approaches full density and the compression modulus reflects the properties of the network. For simplicity, in the following discussion, the load at three different degrees of compression (22%, 47%, 50%, shown in Figure 5A as black diamonds, black squares, and open triangles) will be compared rather than the entire curve. These three points represent strains in the viscous plateau range and as the material approaches full density. Figure 5A−C shows these loads as a function of structural variable for the three sets of samples.

For the samples made varying the ratio of high to low molecular weight chains [Figure 5A], the load at low compressive strain decreases slightly from 200 kPa with increasing HMW chains. The loads at the mid compressive strain (47%) remain roughly constant at 600 kPa until ∼ 84% HMW chains where the required load begins to decrease for increased content of the HMW chains. The loads at high compressive strain (50%) increase from 700 kPa at a content of 77% to 800 at 84% and then decrease to 400 kPa at 86.5%. For the samples made with varying amounts of the high functionality [$\phi = 60$] cross-linking PMHS [Figure 5B], the loads at all compressive strains steadily increased as the amount of PMHS was increased from 2 to 6 wt %. As the degree of compression increases from 22% to 50% the slope of the data increases. For the samples made with increasing functionality of the PMHS site [Figure 5C], the loads at all compressive strains steadily increase with increased functionality. Again, the degree of increase for the different compressive strains increases with the compressive strain, though less severely than for the PMHS content study.

Nonstoichiometric networks imply a high amount of dangling chain ends, which may be expected to affect the material mechanical properties. However, we have observed no changes in the mechanical properties that could be directly attributed to the stoichiometric ratio. This is not necessarily surprising given that most of the highly functional junctions in the networks prepared here still have a significant fraction of chains branching off that can interact with the network. Also, the molecular weights of the high and mid MW chains are well above the critical MW for entanglements ($M_e \sim 8100-12000$ g/mol).[5,26] As a result, they would be expected to contribute to the mechanical properties, although to a lesser degree than chemical cross-links.[4,6,7]

The percent change in $1/T_2$ (the sol-fraction T_2 remained constant at ∼12 ms and the content remained constant within experimental error at 4 ± 2% for all samples) as measured by spin-echo methods for the three studies are shown in Figure 5D−F. As the amount of the low cross-link density chains increased, $1/T_2$ remained constant, within error. As the amount of PMHS increased, $1/T_2$ increased; and as the MW of the PMHS increased, $1/T_2$ increased until $\phi = 70$ then $1/T_2$ is lower for $\phi = 80$. The spin-echo curves here do not show any evidence of the mixed-Gaussian/Exponential decay shapes typical for cross-linked silicones and did not show any evidence for more than two components (the network component ($T_2 \sim 1.5$ ms) and the sol-fraction ($T_2 \sim 12$ ms)).[17]

Cross-link density was measured indirectly by the mass increase upon swelling in toluene. The percent change in cross-link density as measured by percent increase in weight from swelling in toluene are shown in Figure 6G−I. The cross-link density was observed to decrease to a small extent with increased amount of high molecular weight chains. For samples prepared with varying amounts of PMHS, it was observed that the amount of toluene swelling decreased with an increase of PMHS. For samples with increasing functionality of the PMHS cross-linker, the cross-link density steadily increased, as would be expected with an increase in the number of chemical cross-link junctions. For all samples the trends observed in the mechanical properties, the swelling, and the spin-echo experiments are similar, with the exception of the sample with $\phi = 80$. The data shown here underline the need for characterization tools that provide insight into domain distributions. While average cross-link density can be estimated from these methods no characterization of changes in distributions between domains can be obtained. Such changes

Table 2. Results of Analysis of ^{1}H Spin-Echo and ^{1}H Multiple Quantum Build-up Curves for Samples Studied Here[a]

						2-component fit			FTIKREG distribution deconvolution				
study	sample	% PMHS	PMHS ϕ	% HMW PDMS	T_2 (ms)	$\langle\Omega_d\rangle_{low}$ (krad/s)	$\langle\Omega_d\rangle_{high}$ (krad/s)	X_{low}	$\langle\Omega_d\rangle_{low}$ (krad/s)	$\langle\Omega_d\rangle_{high}$ (krad/s)	σ_{low}	σ_{high}	X_{low}
PDMS content	SX4	4	60	77.1	1.61	1.00	4.64	0.66	0.78	5.3	0.48	2.13	0.91
	SX462	4	60	83.8	1.61	1.09	5.14	0.69	0.92	4.6	0.37	0.79	0.91
	SX464	4	60	86.5	1.66	1.14	5.07	0.71	0.93	3.9	0.38	0.57	0.93
	SX466	4	60	89.2	1.66	1.06	5.32	0.73	0.88	4.3	0.37	0.74	0.92
PMHS content	SX2	2	60	77.1	1.80	1.04	3.81	0.70	0.92	4.3	0.38	1.42	0.90
	SX3	3	60	77.1	1.58	1.14	5.32	0.70	0.96	3.7	0.35	0.89	0.81
	SX3.5	3.5	60	77.1	1.56	1.17	5.32	0.70	0.90	5.5	0.39	1.47	0.89
	SX4	4	60	77.1	1.61	1.00	4.64	0.66	0.78	5.3	0.48	2.13	0.91
	SX4.5	4.5	60	77.1	1.52	1.08	5.07	0.67	0.95	5.6	0.43	2.42	0.87
	LK3626	6	60	77.1	1.44	1.18	6.84	0.65	0.97	6.2	0.48	2.05	0.89
PMHS mol wt	LK(short)	6	30	77.1	1.53	1.19	7.29	0.73	0.98	3.1	0.52	0.83	0.96
	LK3626	6	60	77.1	1.44	1.18	6.84	0.65	0.97	6.2	0.48	2.05	0.89
	LK(DC)	6	70	77.1	1.32	1.14	5.61	0.58	0.94	3.9	0.46	0.90	0.88
	LK(UCT)	6	80	77.1	1.46	0.97	5.24	0.56	0.78	3.6	0.36	0.94	0.84

[a] ϕ = number of functional sites.

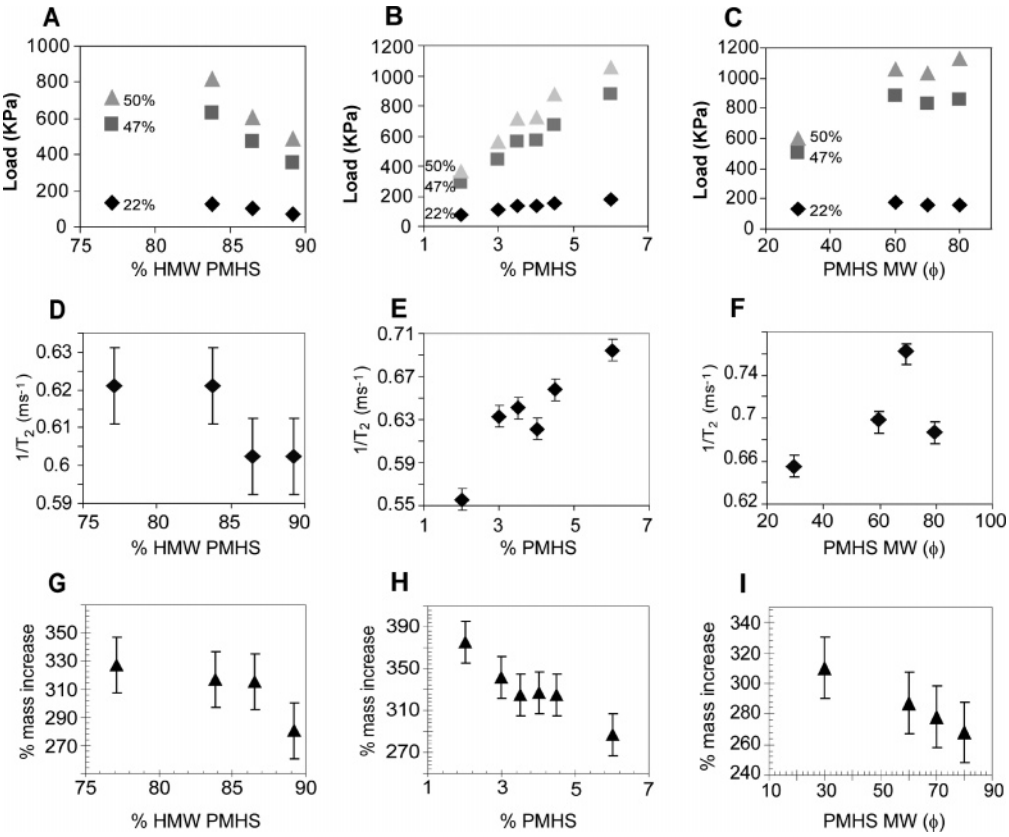

Figure 5. Results of load retention testing (A−C), spin-echo (D−F) and swelling (G−I) analysis of the samples studied here. Key: (A) load at the indicated compressive strains for samples synthesized with varying amounts of high molecular weight vs low molecular weight chains; (B) load at indicated compressive strains for samples synthesized with varying amounts of the highly functional cross-linking site PMHS; (C) load at the indicated compressive strains for samples synthesized with increasing MW of the PMHS cross-linking chains. (D−F) results of analysis of spin-echo decay curves for same samples. (G−I) % increase in mass after swelling in toluene for same samples in parts A−C.

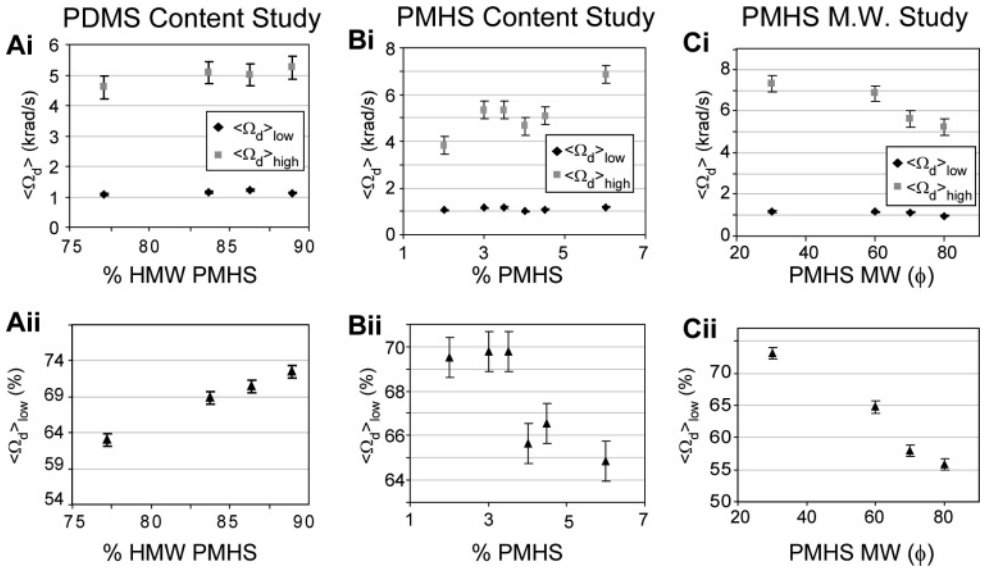

Figure 6. Results of deconvolution of MQ growth curves for all samples studied here to eq 4 with two sites plotted as a function of synthesis variable. $\langle\Omega_d\rangle_{high}$ is for the PDMS chains with high cross-link density, while $\langle\Omega_d\rangle_{low}$ is for PDMS chains with low cross-link density (see text).

in domain size or distribution can be key contributors to mechanical property changes.

The MQ growth curve obtained for a representative sample (LK3626) is shown in Figure 3A. Fits to one $\langle\Omega_d\rangle$ were unable to acceptably fit the growth curve for any sample studied here (though, with the exception of the sol fraction which is not measured in the MQ experiments, the spin-echo methods only detected a single bulk T_2). In order to obtain an acceptable fit, a growth curve obtained from a superposition of two growth curves was necessary. A bimodal growth curve derived from a domain with $\langle\Omega_d\rangle_{low}$ of near 1200 rad/s (population 65%) and a domain with $\langle\Omega_d\rangle_{high}$ of near 6900 rad/s (population 35%) was obtained from a least-squares fit of eq 4 is indicated by the dashed line in Figure 3A. The MQ growth curves for each domain are also shown in Figure 3A. Previous studies have observed such bimodal growth curves and they have been assigned to network domains with low cross-link densities and high cross-link densities. These can be due to heterogeneous

network structure or interactions with the filler interface.[22,26] For these samples, we assign the $\langle\Omega_d\rangle_{low}$ domain to high and mid molecular weight network chains far from the highly functional PMHS cross-linking sites, and the $\langle\Omega_d\rangle_{high}$ domain to the low molecular weight chains and the chains near the PMHS highly functional cross-linking species. These assignments are based on the following justifications: the filler content is low (15 wt % of diatomaceous earth, surface area $\sim$ 10 m^2/g); thus, the amount of adsorbed chains would be expected to be negligibly small (<1%). The populations derived from the bimodal model, 65% low cross-link density chains and 35% high cross-link density chains, are very similar to those derived from the starting materials, 16.5 wt % low MW chains, 13.9 wt % mid MW chains, and 41.6 wt % high MW chains. Neglecting the contribution of chains near the PMHS cross-linking sites results in a prediction of 77% of ^{1}H spins in the $\langle\Omega_d\rangle_{low}$ and 23% in the $\langle\Omega_d\rangle_{high}$ domain. Taking the extra 12% in the $\langle\Omega_d\rangle_{high}$ domain to be monomers of the polymer chains attached to the PMHS cross-linking sites, we predict that the first four monomers of each chain are constrained such that their residual dipolar coupling increases to values similar to $\langle\Omega_d\rangle_{high}$.

Results of the discrete two site fit to eq 4 are listed in Table 2 and plotted as a function of structural variable changed in Figure 6. For the set of samples prepared with varying amounts of high MW chains to low MW chains, $\langle\Omega_d\rangle_{low}$ remained constant at $\sim$1 krad/s while $\langle\Omega_d\rangle_{high}$ increased steadily from 4.5 to 5.5 krad/s. The percentage of chains in the $\langle\Omega_d\rangle_{low}$ domain also increased steadily from 63% to 73%. For the series prepared with increasing PMHS content, again $\langle\Omega_d\rangle_{low}$ remained constant at $\sim$ 1 krad/s while $\langle\Omega_d\rangle_{high}$ increased from 4 to 7 krad/s and the percentage in $\langle\Omega_d\rangle_{low}$ decreased from 70% to 65%. In the series of samples prepared with increasing functionality of the PMHS cross-linking agent, $\langle\Omega_d\rangle_{low}$ remained constant at 1 krad/s, $\langle\Omega_d\rangle_{high}$ decreased from 7 to 5 krad/s, and the population in $\langle\Omega_d\rangle_{low}$ decreased from 75% to 55%.

MQ growth curves as obtained here can also be described by distributions of residual dipolar couplings.[19] Attempts to fit the growth curves obtained in this study to a single Gaussian site were unacceptable in all cases and are not presented. As described here in the Experimental section and described by Saalwächter, the MQ growth curves can also be analyzed by regularization.[26] The result from FTIKREG regularization of the LK3626 sample is shown in Figure 3B and shows two broad distributions of residual dipolar couplings centered near 1 and 4 krad/s, similar to the $\langle\Omega_d\rangle$ obtained from the two site fits. The result of the FTIKREG regularization were then fit to overlapping Gaussian peaks as described in the Experimental Section, and the width and relative populations of the two sites were obtained with $X_{low} = 89\%$, $\sigma_{low} = 0.48$, and $\sigma_{high} = 2.05$. The distributions of $\langle\Omega_d\rangle$s obtained through regularization indicate that, in general, two Gaussian functions can describe the build up curve as shown in Figure 3B. The technique of regularization followed by peak fitting also proved to be a far more efficient than fitting multiple Gaussian functions with MatLab. The results of regularization followed by deconvolution are listed in Table 2 and plotted as a function of structural variable in Figure 7.

Figure 7Ai shows the change in $\langle\Omega_d\rangle_{low}$ and $\langle\Omega_d\rangle_{high}$ with increasing content of the high molecular weight chains and Figure 7Aii shows the change in the partitioning between the two sites as a function of increasing High MW PDMS chain content. For this series of samples, we observed that, as the PDMS content was increased, $\langle\Omega_d\rangle_{low}$ remained relatively constant and the number of chains that could be described by

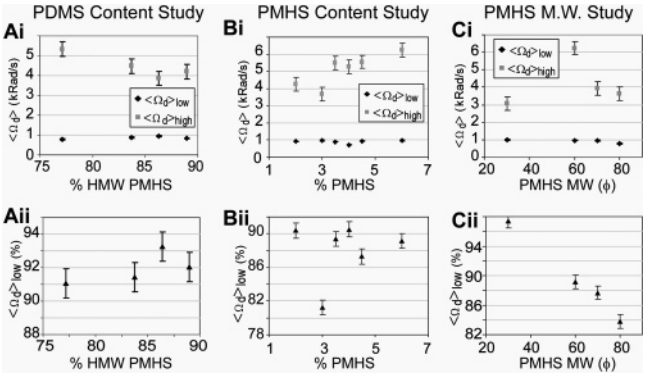

Figure 7. Results of deconvolution of MQ growth curves for all samples studied here using FTIKREG regularization and fitting with FitYK as a function of synthesis variable. $\langle\Omega_d\rangle_{high}$ is for the PDMS chains with high cross-link density, while $\langle\Omega_d\rangle_{low}$ is for PDMS chains with low cross-link density (see text).

$\langle\Omega_d\rangle_{low}$ was also constant. The width in the distributions of $\langle\Omega_d\rangle_{high}$ and $\langle\Omega_d\rangle_{low}$ decreased generally as the number of HMW chains increased with the width in the distribution of $\langle\Omega_d\rangle_{high}$ decreasing to a greater extent (see Table 2). The results of the deconvolution of the $\langle\Omega_d\rangle$ distributions for the samples prepared with increasing PMHS content are presented in Figure 7, parts Bi and Bii. As the PMHS content was increased, $\langle\Omega_d\rangle_{low}$ remained fairly constant at $\sim$ 1 krad/s, while an increase in $\langle\Omega_d\rangle_{high}$ from 4.2 to 6 krad/s and the amount of protons with $\langle\Omega_d\rangle_{low}$ remained constant. The width in the distributions of $\langle\Omega_d\rangle_{high}$ and $\langle\Omega_d\rangle_{low}$ were observed to increase for this series of samples as the PMHS content was increased, again with $\langle\Omega_d\rangle_{high}$ changing to a higher degree than $\langle\Omega_d\rangle_{low}$ (see Table 2). The results of the deconvolution of the $\langle\Omega_d\rangle$ distributions for the samples prepared with increasing PMHS molecular weight and functionality are presented in Figure 7, parts Ci and Cii. As the MW of the PMHS increased, the average $\langle\Omega_d\rangle_{high}$ increased from 3 to $\sim$ 4 krad/s (the sample with $\phi = 60$ was found to be much higher at 6.2 krad/s), the $\langle\Omega_d\rangle_{low}$ remained constant at 1 krad/s and the population in $\langle\Omega_d\rangle_{low}$ decreased from $\sim$ 95% to 83%. The widths of the distributions in both $\langle\Omega_d\rangle_{high}$ and$\langle\Omega_d\rangle_{low}$ were observed to remain constant for the most part with changes in the MW of the PHMS component, with the exception of the LK3626 sample with $\phi = 60$. For this sample, $\langle\Omega_d\rangle_{high}$ and the width of $\langle\Omega_d\rangle_{high}$ were observed to be higher than other samples in this set, though in line with the trends observed in the PMHS content study. It is unknown at this time what is the cause of this discrepancy, but could be due to processing differences in the MW study.

The values of $\langle\Omega_d\rangle$ obtained from regularization are all slightly lower than those obtained with the two-component fit, while the percentages of $\langle\Omega_d\rangle_{low}$ are about 20% higher. However, comparisons of the FTIKREG data in Figure 7 with the two component fits in Figure 6 show that the trends remain similar. One exception to this is the PDMS content study in which no trends, either in the values of $\langle\Omega_d\rangle$ or in the percentages of the components, are seen in Figure 7, parts Ai and Aii. For the PMHS content study the higher $\langle\Omega_d\rangle$ increases with increasing amounts of PMHS, shown in Figure 7Bi, which is consistent with the previous two-component results. For the PMHS MW study, Figure 7Cii shows a distinct trend of a decrease in the percentage of sites characterized by the lower $\langle\Omega_d\rangle$ with increasing molecular weight. However, the trend seen in the two-site fitting, where the higher $\langle\Omega_d\rangle$ decreased, was not seen in the distribution's deconvolutions.

It has been pointed out previously by Saalwächter that the distributions obtained by the regularization of the MQ growth

Table 3. Results of Deconvolution of MQ NMR Experiments on Pristine and Swollen SX2 and LK3626 Sample. Two Site Fit to Equation 4 and FTIKREG Distribution Deconvolution Based on Two Gaussian Distributions in the Dry Case and a Gaussian (low Frequency) and Γ Distribution (high Frequency) for Swollen Case (See Text)

		2-component fit			FTIKREG distribution deconvolution				
sample		$\langle\Omega_d\rangle_{low}$ (krad/s)	$\langle\Omega_d\rangle_{high}$ (krad/s)	X_{low}	$\langle\Omega_d\rangle_{low}$ (krad/s)	$\langle\Omega_d\rangle_{high}$ (krad/s)	σ_{low}	σ_{high}	X_{low}
SX2: 2 wt % PMHS	dry	1.04	3.81	0.70	0.92	4.3	0.38	1.42	0.90
	swollen in toluene-d_8	0.75	3.77	0.57	0.66	2.60	0.37	2.13	0.66
LK3626: 6 wt % PMHS	dry	1.18	6.86	0.65	0.97	6.2	0.48	2.05	0.89
	swollen in toluene-d_8	0.85	4.67	0.55	0.79	2.88	0.60	2.35	0.79

curves are only semiquantitative.[26] However, some key observations can be made. Similar to other PDMS networks studied to date by these MQ methods, the distributions found here are narrower than would be expected from a Gaussian distribution of chain end-to-end distances. The widths observed here, though, are broader than those found in the mono- and bimodal networks studied by Saalwächter.[26,30] Further, qualitative conclusions can be made within a family of samples from the width of the distributions. Of particular interest in this study, for example, is the increase in both the average value of $\langle\Omega_d\rangle_{high}$ and the width in both $\langle\Omega_d\rangle_{high}$ and $\langle\Omega_d\rangle_{low}$ with increasing PMHS content. Interestingly, as the amount of the PMHS increases from 2 to 6 wt %, the amount of $\langle\Omega_d\rangle_{high}$ chains did not appreciably change as might be expected. Since $\langle\Omega_d\rangle$ originates from both the number of segments between constraints and the distributions in the orientation of the end-to-end vector, **R**, the data reported here suggests that the PMHS multifunctional cross-linking sites increase local ordering presumably due to mutual chain packing in the cross-linking area and due to the increased likelihood that chains will be terminated at each end by the PMHS sites. Of final note: given the increased complexity of the analysis via regularization compared to the two site method, it may be, in general for PDMS polymers, favorable to employ the two site models for analysis of network properties.

The values of the residual dipolar couplings obtained in this study compare well with values obtained elsewhere given the differences in network structure.[33] From eq 5, the dynamic order parameters observed here are $S_{b,low} \sim 0.035$ and $S_{b,high} \sim 0.16$. These values lead to average *N*, number of NMR-active submolecules, of 17 and 4, respectively. Previous studies have estimated the number of monomers per statistically relevant submolecule to be ~ 5.85.[43] This would estimate molecular weights between cross-links of $MW_{low} \sim 7500$ g/mol and $MW_{high} \sim 1600$ g/mol. MW_{low} is similar to the estimated MW between entanglements of 8100−12000 g/mol and suggests that the segmental order in this domain is determined not by the chemical cross-links, but by the entanglements. The MW_{high} is in general agreement with the value of the short chain constituent starting material.

For all samples studied here, the MQ NMR approach provides additional insight into the segmental dynamics and segmental ordering that the swelling and the spin-echo methods do not. As mentioned above, the swelling and spin-echo approaches do not allow us in this series of samples to individually characterize the domains with low and high cross-link densities and provide only a bulk average measure of the cross-link density. The MQ NMR methods, on the other hand, have allowed us to measure the residual dipolar couplings in both domains selectively. These measurements provide key insight into the segmental ordering (see eq 5) and provide additional insight into the contributions of each domain to the mechanical properties. As shown in Figure 4 and 5, the modulus at low % compression is fairly constant for all samples while the modulus at high % compression is very sensitive to the synthetic variables. The MQ results on these samples indicate that the residual dipolar coupling of the domains with low cross-link density are fairly unchanged with changes in the composition of the polymer network while the residual dipolar couplings of the domains with high cross-link density are strongly correlated with the compositional variables. Comparing the compression results with the results of the MQ NMR studies indicate that the material mechanical properties at high compression are influenced by the segmental structure of the domains with high cross-link density, as has been suggested in previous studies.[9−11]

Numerous theories have been developed to predict the heterogeneous "nonaffine" deformation of bimodal networks under strain.[9−11] Our experimental setup did not allow for controllable in-situ MQ NMR analysis of the materials studied here under compressive strain. Saalwächter recently showed that in situ-MQ NMR is conveniently performed on samples strained during solvent swelling.[27] [Previous studies have used spin-echo methods on swollen samples.[44,45]] The MQ-NMR growth curves and the regularization of those growth curves for samples SX2 and LK3626, unswollen and swollen in toluene-d_8, are shown in Figure 8. These samples are identical except for the amount of the highly functional cross-linking site PMHS [2 wt % for SX2, 6 wt % for LK3626]. Similar to Saalwächter's results, the data shown here indicates that upon swelling, the average segmental order increased, as can be seen from the increased growth rate of the MQ signal (Figure 8A). Results of a discrete two site fit to eq 4 are shown in Table 3. Distributions obtained from FTIKREG regularization are shown in Figure 8, parts C (SX2) and D (LK3626). The results of the deconvolution of the distributions for the dry samples are shown in Table 1. For the swollen samples, we were unable to fit the distributions by two Gaussian or split Gaussian distribution functions. As shown in Figure 8B, acceptable fits were obtained, however, for a split-Gaussian for $\langle\Omega_d\rangle_{low}$ and a Γ distribution for $\langle\Omega_d\rangle_{high}$. Results of these deconvolutions are shown in Table 3.

For SX2, the mean frequency of the low-frequency narrow distribution, $\langle\Omega_d\rangle_{low}$, was observed to decrease slightly from 1.04 to 0.76 krad/s (discrete two site fit). For LK3626, the mean $\langle\Omega_d\rangle_{low}$ was observed to decrease slightly from 1.18 to 0.85 krad/s (discrete two site fit). Similar trends were observed in the mean $\langle\Omega_d\rangle_{low}$ obtained from requlariation. For SX2 the width of the distribution in $\langle\Omega_d\rangle_{low}$ was observed to remain unchanged, while for LK3626 an increase of 20% was observed, consistent with heterogeneous deformation. The reduction in $\langle\Omega_d\rangle_{low}$ is consistent with some increase in mobility upon swelling. For both samples, the changes observed in $\langle\Omega_d\rangle_{low}$ are significantly less than what would be predicted for affine deformation by eq 7 ($Q_{SX2} \sim 3.7$; $Q_{LK3626} \sim 2.9$):[27]

$$\langle\Omega_d\rangle_{swollen} = \langle\Omega_d\rangle_{dry} Q^{2/3} \tag{7}$$

Similar results on bimodal networks were observed by Saalwächter and were attributed to desinterspersion processes.[27]

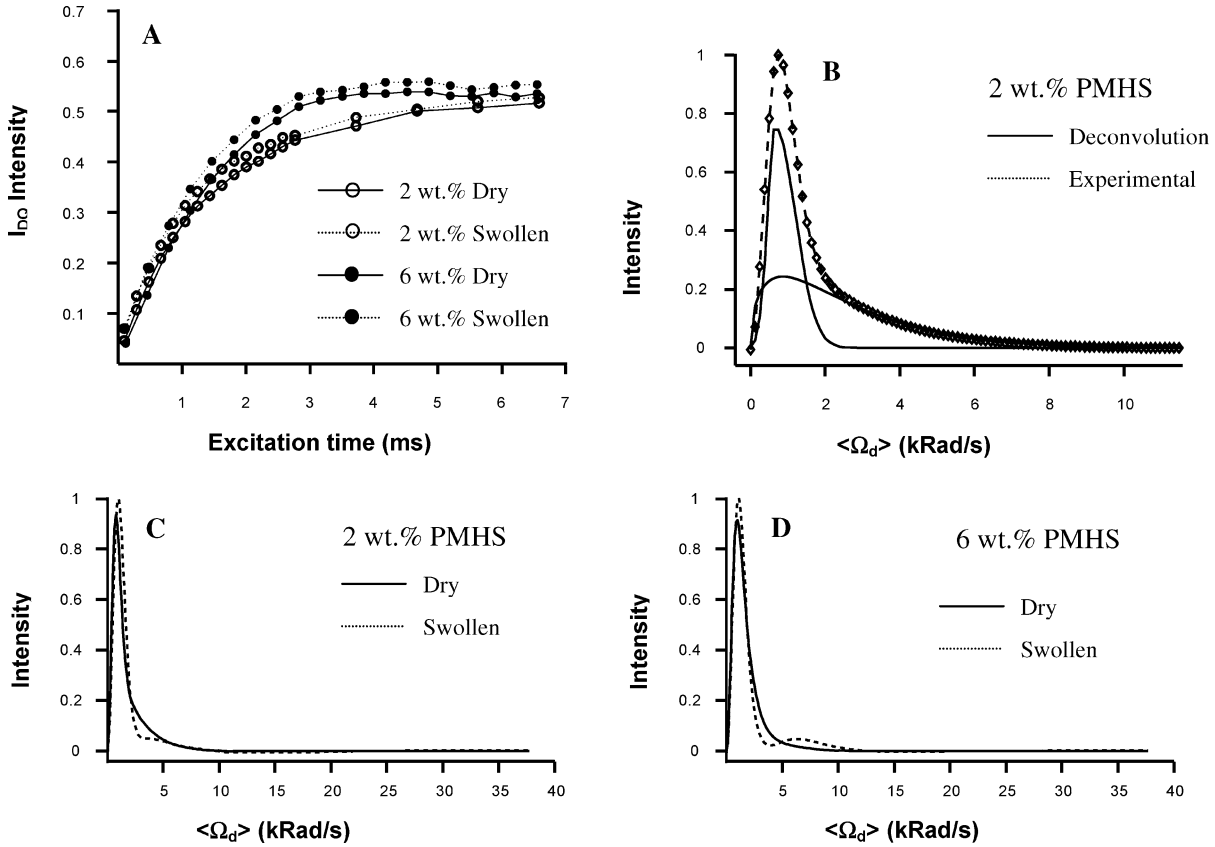

Figure 8. (a) Normalized DQ buildup curves of SX2 (2 wt % PMHS) and LK3626 (6 wt % PMHS) for both dry and swollen samples in toluene-d_8. (b) Distribution of residual dipolar couplings from FTIKREG regularization and fitting with FitYK. Solid lines are the fits of Gaussian and Γ line shapes to the two overlapping distributions. Dashed line is the overall fit obtained by summing the two distributions. Distributions of RDCs are explicitly shown for dry and swollen (shown in dashed and solid lines respectively) samples of (c) SX2 and (d) LK3626.

For the high-frequency reservoir, the mean residual dipolar couplings obtained from the discrete two site fit were observed to increase for both LK3626 and SX2, though for SX2 the increase was marginal. In both cases, the increase was significantly less than would be predicted from eq 7 for affine deformation (predicted: $\langle\Omega_d\rangle_{high-LK3626} \sim 9$ krad/s; $\langle\Omega_d\rangle_{high-SX2} \sim 11$ krad/s). The distributions obtained from regularization interestingly, did not show an obvious, discrete high-frequency population for either sample. The distributions, however, could not be fit to fewer than three discrete overlapping Gaussian distributions. In fact, the only reasonable fit obtainable for the distributions was obtained using a Gaussian distribution for the low-frequency component and a Γ distribution for the high-frequency component:

$$P(|\langle\Omega_d\rangle|) = \frac{2}{\sqrt{\pi}}\sqrt{\frac{|\langle\Omega_d\rangle|}{\xi^3}}\, e^{-\frac{|\langle\Omega_d\rangle|}{\xi}} \tag{8a}$$

$$\xi = \frac{2|\langle\Omega_d\rangle_{static}|}{5N}\,|\langle P_2(\cos\alpha)\rangle| \tag{8b}$$

$$\overline{\langle\Omega_d\rangle} = \frac{3}{2}\xi \tag{8c}$$

$$\sigma^2 = \frac{3}{2}\xi^2 \tag{8d}$$

where $\overline{\langle\Omega_d\rangle}$ and σ^2 are the mean RDC and variance of the distribution respectively. As noted by Saalwächter, the Γ distribution would be expected from a Gaussian distribution of chain end-to-end vectors and results in a very broad distribution of residual dipolar couplings.[28] [The distributions obtained by the MQ approach used here for most of the PDMS samples studied to date have not been shown to be describable by a Γ distribution and that, in fact, the distributions observed to date, are remarkably narrow.] The distributions obtained by regularization can be subject to systematic errors and to errors from fitting growth curves with finite signal-to-noise, and might only be considered semiquantitative. The results shown here, however, strongly suggest that for the chains describable by a high-frequency residual dipolar coupling, the swelling process is highly heterogeneous, with the heterogeneity increasing with PMHS content. We have assigned the $\langle\Omega_d\rangle_{high}$ chains to chains with low molecular weight between cross-links and to chains near the highly functional cross-linking PMHS sites. If such an assignment is correct, the heterogeneity of the deformation during swelling is understandable, i.e., chains near the cross-linking sites will see significantly more interchain interaction during swelling than chains far away from these sites.

Conclusions

The segmental order and dynamics of polymer network chains in a trimodal silicone network have been studied by static ^{1}H MQ-NMR methods. The MQ-NMR methods have allowed for the quantitation of chains in domains of high and low cross-link density comparable to the concentrations expected from the synthetic starting materials. Three structural variables were systematically varied over a limited range to target a desired set of engineering requirements. The mechanical properties and distributions of residual dipolar couplings were measured in order to gain insight into the network structural motifs that contribute significantly to the composite properties. The results of this study suggest that the domains with high cross-link density contribute significantly to the high strain modulus, while

the low cross-link density domains do not. This is in agreement with theories and experimental studies developed for tensile strain in silicone bimodal networks over the last 20 years. Unfortunately, the theoretical approaches that have been developed to link tensile modulus results to network structural motifs are not valid for compression of porous foam elastomers. This lack of theoretical correlation underlines the important role MQ NMR methods can play in understanding the structure−property relationships in such materials. In situ MQ-NMR of swollen sample suggests that the networks deform nonaffinely, in agreement with previous studies, and heterogeneously. The heterogeneity was observed to be dependent on the amount of the highly functional cross-linking site, PMHS. The NMR experiments shown here provide increased ability to characterize multimodal networks of typical engineering silicone materials and to gain significant insight into structure−property relationships. These tools are of particular value for studying aged, degraded, or unknown samples for which prior insight in to the network structure is unavailable.

Acknowledgment. This work was performed under the auspices of the U.S. Department of Energy by the Lawrence Livermore National Laboratory under Contract No. W-7405-ENG-48. The authors would like to thank Seth Gleiman and Jim Schnieder for their assistance in synthesis, Ed Fuller for GPC analysis of raw materials, and Kay Saalwächter for helpful discussions. Part of this work was supported by the LLNL Laboratory Directed Research and Development (LDRD) program (tracking number: 06-SI-005).

References and Notes

(1) Flory, P. J. *Principles of Polymer Chemistry*; Cornell University Press: New York, 1953.
(2) Bicerano, J. *Prediction of Polymer Properties*, 3rd ed.; Marcel Dekker: New York, 2002.
(3) Van Krevelen, D. W. *Properties of Polymers*, 3rd ed.; Elsevier: Amsterdam, 1997.
(4) Larsen, A. L.; Hansen, K.; Sommer-Larsen, P.; Hassager, O.; Bach, A.; Ndoni, S.; Jorgensen, M. *Macromolecules* **2003**, *36*, 10063.
(5) Seitz, J. T. *J. Appl. Polym. Sci.* **1993**, *49*, 1331.
(6) Andrady, A. L.; Llorente, M. A.; Sharaf, M. A.; Rahalkar, R. R.; Mark, J. E. *J. Appl. Polym. Sci.* **1981**, *26*, 1829.
(7) Gottlieb, M.; Macoscko, C. W.; Benjamin, G. S.; Meyers, K. O.; Merrill, E. W. *Macromolecules* **1981**, *14*, 1039.
(8) Meyers, K. O.; Bye, M. L.; Merrill, E. W. *Macromolecules* **1980**, *13*, 1045.
(9) Mark, J. E. *Macromolecules* **1984**, *17*, 2924.
(10) Mark, J. E. *Acc. Chem. Res.* **1994**, *27*, 271.
(11) Mark, J. E. *Adv. Polym. Sci.* **1984**, *65*, 136.
(12) Llorente, M. A.; Mark, J. E. *Macromolecules* **1980**, *13*, 681.
(13) Kloczkowski, A.; Mark, J. E.; Erman, B. *Macromolecules* **1995**, *28*, 5089.
(14) Bovey, F. A. *NMR of Polymers*; Academic: San Diego, CA, 1996.
(15) Schmidt-Rohr, K.; Spiess, H. W. *Multidimensional solid-state NMR and polymers*; Academic: San Diego, CA, 1994.
(16) Ando, I.; Asakura, T. *Solid State NMR of Polymers*; Elsevier Science: London, 1998.
(17) Cohen-Addad, J. P. *Prog. NMR Spectrosc.* **1993**, *25*, 1.
(18) Gronski, W.; Hoffmann, U.; Simon, G.; Wutzler, A.; Straube, E. *Rubber Chem. Technol.* **1992**, *65*, 63.
(19) Grinberg, F.; Kimmich, R.; Moller, M.; Molenberg, A. *J. Chem. Phys.* **1996**, *105*, 9657.
(20) Chien, A.; Maxwell, R. S.; Chambers, D.; Balazs, B.; LeMay, J. *J Radiat. Phys. Chem.* **2000**, *59* (5−6), 493.
(21) Maxwell, R. S.; Balazs, B. *J. Chem. Phys.* **2002**, *116*, 10492.
(22) Maxwell, R. S.; Chinn, S. C. *Macromolecules* **2005**, *38*, 7026.
(23) Chinn, S. C.; DeTeresa, S.; Shields, A.; Sawvel, A.; Balazs, B.; Maxwell, R. S. *Polym. Deg. Stab.* **2006**, *91*, 555.
(24) Jagadeesh, B.; Demco, D. E.; Blumich, B. *Chem. Phys. Lett.* **2004**, *393*, 416.
(25) Sotta, P.; Deloche, B. *Macromolecules* **1990**, *23*, 1999.
(26) Saalwächter, K.; Herrero, B.; Lopez-Manchado, M. A. *Macromolecules* **2005**, *28*, 9650.
(27) Saalwächter, K.; Kleinschmidt Sommer, J.-U. *Macromolecules* **2004**, *37*, 8556.
(28) Saalwächter, K.; Ziegler, P.; Spyckerelle, O.; Haidar, H.; Vidal, A.; Sommer, J.-U. *J. Chem. Phys.* **2003**, *119*, 3468.
(29) Saalwächter, K. *J. Chem. Phys.* **2004**, *120*, 454.
(30) Saalwächter, K.; Heuer, A. *Macromolecules* **2006**, *39*, 3291.
(31) Wang, M.; Bertmer, M.; Demco, D. E.; Blumich, B.; Litvinov, V. M.; Barthel, H. *Macromolecules* **2003**, *36*, 4411.
(32) Fechete, R.; Demco, D. E.; Blumich, B. *J. Magn. Reson.* **2004**, *169*, 19.
(33) Friedrich, U.; Schnell, I.; Demco, D. E.; Spiess, H. W. *Chem. Phys. Lett.* **1998**, *285*, 49.
(34) Schneider, M. M.; Gasper, L.; Demco, D. E.; Blumich, B. *J. Chem. Phys.* **1999**, *111*, 402.
(35) Graf, R.; Heuer, A.; Spiess, H. W. *Phys. Rev. Lett.*, **1998**, *80*, 5738.
(36) Graf, R.; Demco, D. E.; Hafner, S.; Spiess, H. W. *Solid State NMR* **1998**, *12*, 139.
(37) Fechete, R.; Demco, D. E.; Blumich, B. *Macromolecules* **2002**, *35*, 6083.
(38) Brook, M. A. *Silicon in Organic, Organometallic, and Polymer Chemistry*; John Wiley & Sons: New York, 2000.
(39) Mehring, M. *Principles of High Resolution NMR in Solids*; Springer-Verlag: Berlin, 1983.
(40) Ernst, R. R.; Bodenhausen, G.; Wokaun, A. *Principles of Nuclear Magnetic Resonance in One and Two Dimensions*; Oxford University Press: New York, 1987.
(41) Callaghan, P. T.; Samulski, E. T. *Macromolecules* **2000**, *33*, 3795.
(42) Honerkamp, J.; Weese, J. Fast Tikhonov Regularization (FTIKREG). Freiburger Materialforschunszentrum F.M.F.: Freiburg, Germany, 1992. Weese, J. *Comput. Phys. Commun.* **1992**, *69*, 99.
(43) Kuhn, W.; Grün, F. *Kolloid-Z.* **1942**, *101*, 248.
(44) Cohen-Addad, J. P.; Domard, M.; Lorentz, G.; Herz, J. *J. Phys. (Paris)* **1984**, *45*, 575.
(45) Cohen-Addad, J. P.; Domard, M.; Herz, J. *J. Chem. Phys.* **1982**, *76*, 2744.

MA0620924